LAWRENCE
LIVERMORE
NATIONAL
LABORATORY

UCRL-JRNL-223814

Electron Cloud Measurements in Heavy-Ion Driver for HEDP and Inertial Fusion Energy

M. Kireeff Covo, A. W. Molvik, A. Friedman, R. Cohen, J.-L. Vay, F. Bieniosek, D. Baca, P. A. Seidl, G. Logan, J. L. Vujic

August 18, 2006

Nuclear Instruments and Methods in Physics Research, Section B

ID 397

Electron Cloud measurements in Heavy-Ion Driver for HEDP and Inertial Fusion Energy

Michel Kireeff Covo[1,3], Arthur W. Molvik[1], Alex Friedman[1], Ronald Cohen[1], Jean-Luc Vay[2], Frank Bieniosek[2], David Baca[2], Peter A. Seidl[2], Grant Logan[2], and Jasmina L. Vujic[3]

[1]*Lawrence Livermore National Laboratory, Heavy-Ion Fusion Science Virtual National, Laboratory, Livermore, California 94550, USA*

[2]*Ernest Orlando Lawrence Berkeley National Laboratory, Heavy-Ion Fusion Science Virtual National Laboratory, 1 Cyclotron Road, Berkeley, California 94720, USA*

[3]*University of California at Berkeley, Department of Nuclear Engineering, 4155 Etcheverry Hall, MC 1730, Berkeley, California 94720, USA*

The High Current Experiment (HCX) at LBNL is a driver scale single beam injector that provides a 1 MeV K+ ion beam current of 0.18 A for 5 μs. It transports high-current beams with large fill factor (ratio of the maximum beam envelope radius to the beam pipe radius) and low emittance growth that are required to keep the cost of the power plant competitive and to satisfy the target requirements of focusing ion beams to high-power density. Beam interaction with the background gas and walls desorbs electrons that can multiply and accumulate, creating an electron cloud. This ubiquitous effect grows at higher fill factors and degrades the quality of the beam. We review simulations and diagnostics tools used to measure electron production, accumulation and its properties.

PACS numbers: 29.27.Bd, 29.30.Aj, 34.50.Dy, 41.75.Ak, 79.20.Rf

1. INTRODUCTION

The high-current experiment (HCX) [1] at LBNL is a 1 MeV K^+ linear DC accelerator that produces an ion beam current of 0.18 A for 5 μs from an alumino-silicate surface ionization source. It is the first transport experiment with driver-scale line charge density and pulse duration that has an injector, an electrostatic matching section, an electrostatic transport section and a magnetic transport section (Fig. 1) consisting of four room-temperature pulsed magnetic quadrupoles (QM1-4). The primary goal of the experiment is to study the transport of high-current and high-energy space-charge dominated heavy-ion beams with large fill factors (beyond 60%) and low emittance (~ 0.5 mm mrad for 1σ) growth, in order to reduce the cost of the fusion power plants (minimizing the transport array diameter and in turn the amount of induction core material needed for acceleration) and satisfy the requirements of focusing high-power density for high-energy-density physics (HEDP) and inertial-fusion targets.

If the fill factor is increased, the beam runs closer to the walls and starts to produce secondary electrons and desorbed gas, which could move to the beam path and be ionized. Inside the matching section and electrostatic quadrupole section, the electrons are swept out by the electric field towards the positive rods, but inside the magnetic section, the electrons from the ionization of background and desorbed gas are trapped inside a potential well produced by the space-charge beam potential of ~ 2100 V. The ion-induced electrons desorbed from the walls can also be electrostatically trapped at the beginning of the beam pulse, when the beam potential is rising at a rate of ~ 2000 V/μs, but if they were produced during the flat top, they will reach the walls where they can be lost, and the electron lifetime will be given by its electron yield and reflectivity.

The transverse trapped electrons are confined axially by the suppressor electrode at one end and by the last electrostatic quadrupole electrode at the other end, which are biased to -10 kV and -18.6 kV, respectively. Trapped electrons decrease the beam potential and change the beam envelope, producing a positive feedback that results in electron cloud effects (ECE). Deleterious

ECE include electron-stimulated gas desorption, cloud-induced noise on instrumentation, tune shifts, instabilities and heat deposition on cryocooled components [2].

ECE were observed in the proton storage rings at BINP [3], the intersecting storage rings at CERN [4], the proton storage ring at LANL [5], the relativistic heavy ion collider at BNL [6], the photon factory at KEK [7,8], the low energy ring at KEKB [9], and other storage rings. They can potentially limit the performance of the spallation neutron source at ORNL [10,11], and the large hadron collider (LHC) at CERN [12], and have been subject of and featured in various meetings (EPAC 2004, ECLOUD'04, ICFA-HB2004, HHH2004, PAC05, DIPAC2005, etc).

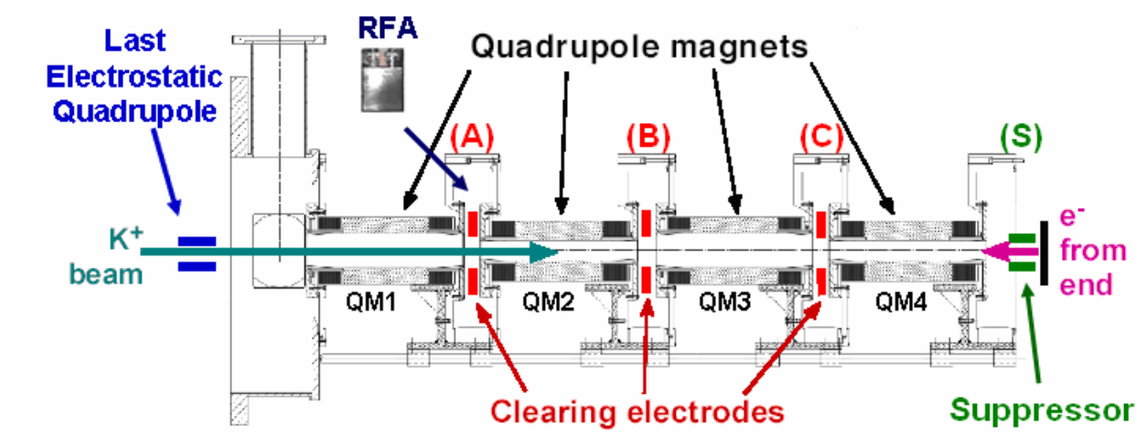

FIG. 1. (Color) Magnetic quadrupole transport section of HCX has 4 quadrupole magnets (QM1-4). Electrons can be confined inside by the beam potential (~ 2100 V), if the suppressor (S) and last electrostatic quadrupole are biased negatively. Local sources of electrons can be removed, if the clearing electrodes (A, B, and C) are turned on. Retarding field analyzer (RFA) measures ions expelled by the beam potential, when the clearing electrode A is taken away.

2. SIMULATIONS

Simulations use the WARP three-dimensional self-consistent particle-in-cell (PIC) code [13]. The code contains a comprehensive set of models governing the interaction of positively-charged beams with stray electron and gas, including secondary electron emission from walls, charge exchange, neutral emission, and other processes. The magnetic transport section from

HCX, Fig. 1, is being used to study ion beams containing electrons, and to validate the WARP code.

A novel mover for electrons that interpolates between full electron dynamics and drift kinetics was developed and implemented in the code. The algorithm is discussed in Ref. [14] and takes advantage of Parker's observation that the conventional Boris particle advance scheme [15], when running with large time steps compared to the cyclotron period, continues to exhibit correct drift velocities, but causes particles to gyrate with a large radius compared to the physical gyro orbit, and with a frequency that is lower than the physical gyrofrequency. This Cohen mover performs an interpolation between full electron dynamics (Boris mover) and drift kinetics (motion along B plus drifts), to preserve the physical gyroradius, but with larger time steps, reducing the computational time by a factor of 10-100 times.

The PIC method for simulation of plasmas and particle beams was also merged with the adaptive mesh refinement (AMR) technique [16]. This technique covers areas that need a higher resolution with a finer mesh, if the areas of the physical domain that need refinement evolve in time, then an automatic redistribution of the refinement applies, saving computational effort in simulations of time-dependent space-charge-limited flow in up to 20000 times with proved numerical convergence.

The Cohen mover and AMR technique have led to large speedups for affordable numerically-converged and accurate results. WARP simulations show that the transverse electron density distributions inside the magnetic quadrupoles depend of the nature of the electron source, Fig. 2. Electrons originating from ion impact on structures at the end of HCX will produce a virtual cathode and can move upstream thought two opposite quadrants, Fig. 2(a), by $\vec{E} x \vec{B}$ and $\nabla \vec{B}$ drifts if the suppressor electrode is turned off. Electrons originating from ionization of background gas will have the beam profile, Fig. 2(b), and the even and odd quadrants will drift in opposite directions. Electrons desorbed from the beam pipe will populate

the entire transverse section, following the magnetic field lines and peaking near the wall at the center of the quadrants, Fig. 2(c).

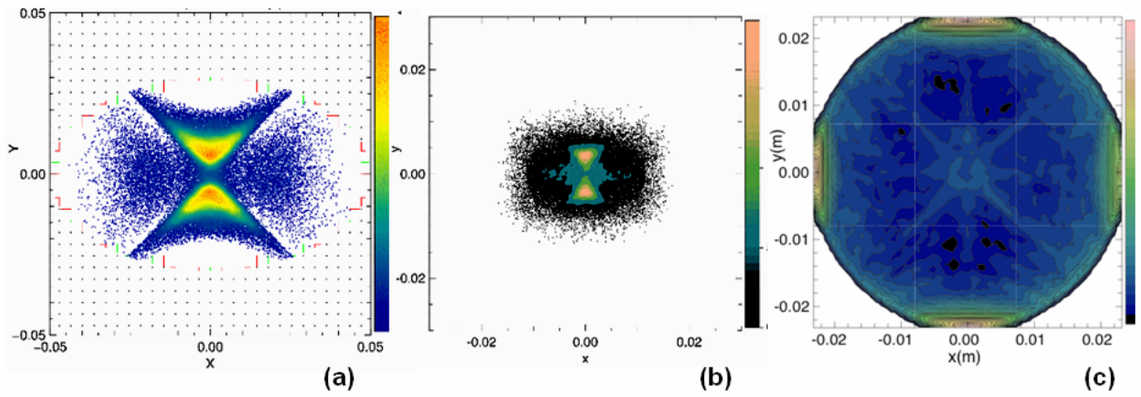

FIG. 2. (Color) Transverse electron density distributions inside the magnetic quadrupoles of HCX. (a) Electrons originating from ion impact on end wall structures. (b) Electrons originating from ionization of background gas. (c) Electrons desorbed from the beam pipe.

3. EXPERIMENTS

The gas-electron source diagnostic (GESD) [17] is an instrumented target to measure ion-induced gas and electron production as a function of the ion angle of incidence. The GESD measured that each 1 MeV K+ ion impacting near grazing incidence on stainless steel desorbs ~ 10,000 molecules of gas and produces ~ 100 electrons. A theoretical model for the electron desorption [18], using TRIM code to evaluate dE_e/dx at several depths in the target, demonstrated good agreement with the experimental data and also models gas desorption [19].

The measured electron and gas desorption yield are needed for calibration of signal intensities collected on the wall electrodes inside the last two magnetic quadrupoles, QM3-4. These set of passive nonintercepting diagnostics include flush probes, capacitive probes and gridded probes [17,20]. All the electrodes have dedicated coupling circuits to simultaneously permit biasing and measuring small currents, using current ampilifiers. The amplified signals are digitalized by an A/D converter, and analyzed and archived by a Labview program.

The third quadrupole magnet has an array of 8 long flush collectors (FLLs), Fig. 3. These electrodes are mounted longitudinally on the beam bore pipe, the array encircles the beam with a length exceeding the effective magnetic field of the quadrupole. The FLL signal is a sum of the beam loss, the secondary electrons and the induced charge by the ion beam. The beam loss is negligible compared with the secondary electrons emitted and can be neglected. The design was made in such way that the magnetic field lines through one electrode will go through the adjacent electrode. The paired electrodes that share the same transverse magnetic field lines have opposite bias ($\pm$ 50 V). Ion-induced electrons from the negatively biased flush electrode inside the quadrupole will follow the magnetic field lines and end up in the positively biased electrode. Ideally, measurement of ion-induced electron emission from the negatively biased probes can be made by summing the differences between paired electrodes, which removes the capacitive signal, and dividing by two, which takes into account that the electron current leaving one electrode is collected by its pair. If the bias is inverted and the same procedure is followed, the total ion-induced electron can be obtained by adding up the measured currents for each bias. The beam induced capacitive signal can be obtained by adding the paired signals. In this way, the electron current for the paired probes will cancel out, leaving only the capacitive pickup. Beam loss and the dynamic density of desorbed gas can also be inferred from the total electron emission from the FLLs.

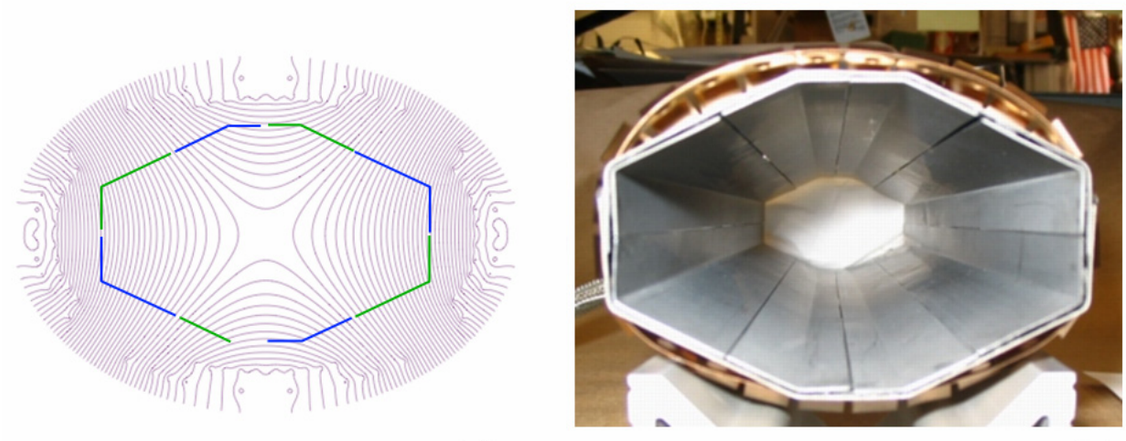

(a) (b)

FIG. 3. (Color) Third magnetic quadrupole - QM3 (a) Transverse magnetic field lines are superimposed to the FLL diagnostics sketch. The green and blue diagnostics that share the same magnetic field lines are called paired. (b) Picture of the diagnostics before the installation.

The fourth quadrupole magnet has three beam position monitors (BPMs), two gridded electron collector (GECs), two gridded ion collectors (GICs), and two short flush collector (FLSs).

The BPMs are recessed from the bore beam pipe and have small scrappers upstream to intercept ions near grazing incidence, before they reach a BPM. They are placed in a region where the magnetic field is parallel to the probe surfaces, magnetically suppressing electron emission. As with any capacitive electrodes, they are sensitive to changing electric fields, which are highest at the head and tail of the beam. The net charge per unit length is obtained by integrating the induced signal and scaling to the probe azimuthal angle and lenght relative to the beam. As electrons decrease the net beam charge, the BPM might determine the density of electrons. A problem was observed because the net induced charge measured does not go back to zero at the end of the beam pulse, probably indicating that some ion-induced electrons escape along magnetic fields to the border. Design modifications to fix this problem are being studied.

The GEC electrodes are recessed from the bore beam pipe behind flush grids and are placed in a region where the magnetic field that passes through the beam enters the electrode. The entrance double grid attenuates the pickup capacitive signal by a factor of ~500, allowing measurements of untrapped electrons expelled at the end of the beam, when the beam potential decays.

The GICs are similar to the GECs but are placed in a region where the magnetic field is parallel to the collector surface, suppressing electron emission or collection. Ions produced from beam-background gas interaction (ionization and charge exchange) are driven across the magnetic field (B’ ~ 8 T/m) by the beam space-charge potential. The entrance double grids

attenuate the capacitive pickup by a factor of 500, enabling measurement of very small expelled ion currents. These gridded electrodes were successfully used to measure the dynamic gas density within the ion beam, effectively an in-situ fast ionization gauge [20].

The FLSs are mounted flush to the beam bore pipe, but they are not paired and have shorter length. The ion-induced electrons can leave the negative electrode and follow the magnetic field lines. Similarly to the long flush probes, they can be calibrated with the GESD data to infer beam loss, and dynamic density of desorbed gas.

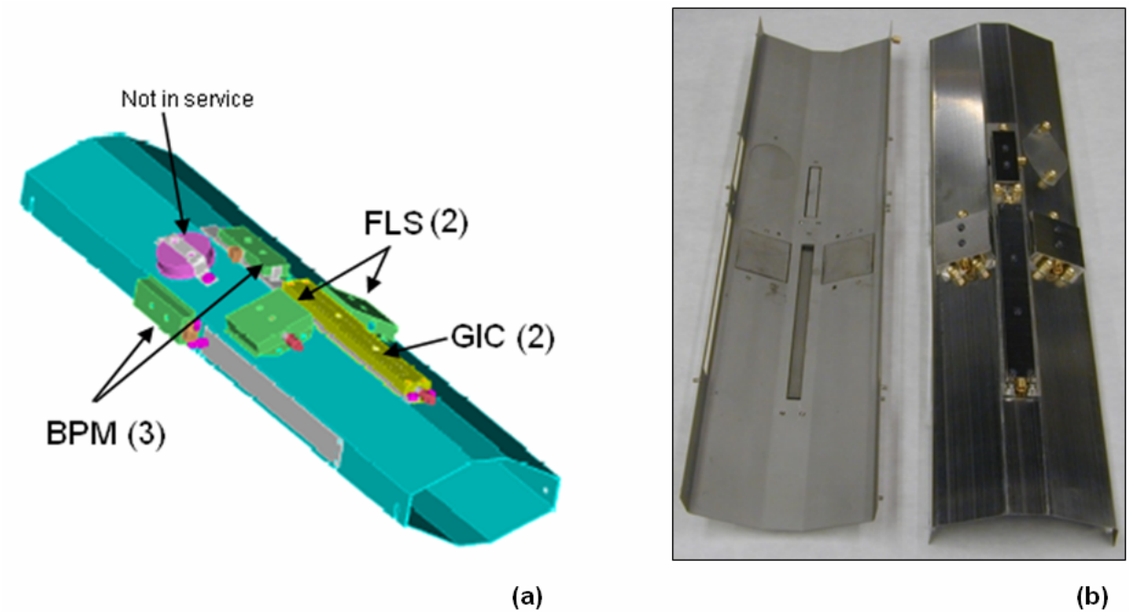

FIG. 4. (Color) Fourth magnetic quadrupole – QM4 (a) Diagnostic sketch showing three beam monitors (BPMs), two gridded ion collectors (GICs), and two short flush collector (FLSs). One BPM and two gridded electron collector (GECs) are placed on the far side and are not seen in the sketch. (b) Picture of the diagnostics before the installation.

Several diagnostics [one suppressor ring, three clearing electrodes, one retarding field analyzer (RFA), one CCD camera, and two Faraday cups] are placed before, after and between the quadrupole magnets and help to study the electron cloud features.

The suppressor ring is installed after the magnetic section. It can be be biased to -10KV, so we can choose to suppress electron emission from K^+ ion impact on end structures.

The clearing electrodes are added to the lattice between magnets. They are stainless steel rings biased positively (+9 kV) to remove electrons that reach the gaps. The clearing electrodes constitute an efficient mitigation technique [20] and can be used to measure electron cloud line charge density at gap A [21]. The static background cloud line-charge density is obtained if the electron current measured with the clearing electrode is divided by the average drift velocity of electrons inside the magnets (~0.60 m/μs) [22].

The RFA, which is a high-pass energy filter with an energy resolution ($\Delta E/E$) of ~ 0.5 %, can be inserted in the drift region between quadrupole magnets QM1-2 (gap A) instead of clearing electrode A. It was adapted from Rosenberg's design [23] that simplified construction through use of commercial parts. The design includes: an extra grid that allows measurements of either ions or electrons that cross the aperture, larger gaps to permit higher electrode bias, and a compact 5 cm linear motion feedthrough for positioning the RFA. It is described in detail in Ref. [24]. The RFA and the clearing electrodes measurements can be combined to provide absolute time-dependent electron cloud density accumulation during the beam pulse [21]. The beam-background gas interaction produces cold ions from ionization and charge exchange that are expelled by the beam space-charge potential, converting potential energy to kinetic energy. The expelled ions reach the walls in few hundred nanoseconds. As electrons accumulate, the beam potential decreases and so does the energy of the expelled ions [25]. The electron density as a function of time is obtained from the beam potential decay measurement accounting for the ion and electron transverse distributions. The dynamic density can be supplemented and corroborated by the static background density obtained from clearing electrodes measurements, giving the absolute electron density.

Ref. [21] describes an experiment that compared the neutralization (ratio of electron to the ion charge density) measured with the RFA and the clearing electrode techniques for three

different conditions. For the first condition (B,C, and S on) the clearing electrodes and the suppressor are all on, minimizing all source of electrons. For the second condition the clearing electrodes are off and the suppressor is on (B,C off and S on), which allows electrons from local sources (ionization and desorbed from the beam pipe) to accumulate. For the third condition the suppressor and the clearing electrodes are off (B,C, and S off), which also allows electrons originating from the end structures to drift upstream. The RFA, Fig. 5(a), and the clearing electrode measurements, Fig. 5(b), give the neutralization shown in Table 1, showing reasonable agreement. The RFA is a versatile tool that also provides information of ion and electron energy distributions, beam potential distribution, halo losses and beam-background gas cross-sections.

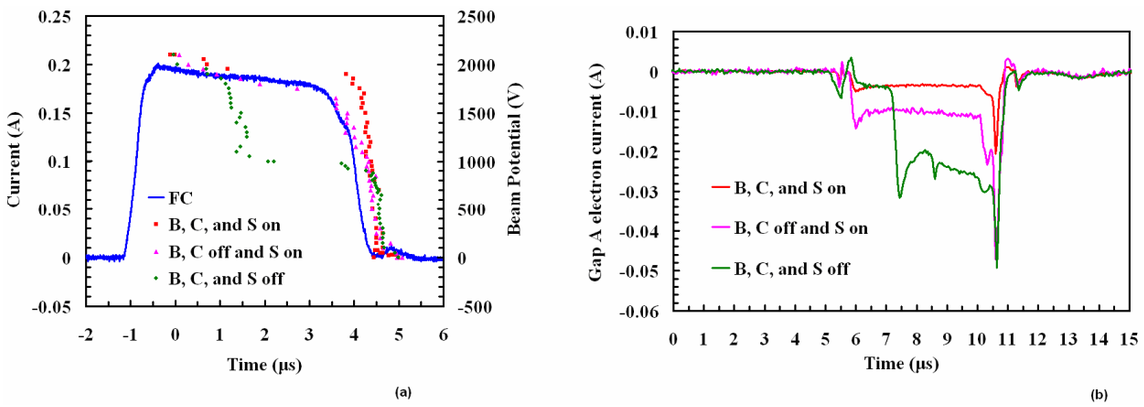

FIG. 5. (Color) (a) Faraday cup current and dynamic beam potential measured for three different configurations, increasing the sources of electrons. For the first condition (B, C, and S on), the clearing electrodes B, C and suppressor are on. For the second condition (B, C, off and S on), we allow local sources of electrons to accumulate by turning off the clearing electrodes B and C. For the third condition (B, C, and S off) we also allow electrons generated at the end structures to drift upstream by turning off the suppressor. (b) Electron current from clearing electrode A obtained for the same configurations of Fig. 3 (a), after subtracting the beam induced capacitive signal.

TABLE 1. Comparison of the beam neutralization measured in gap A using the clearing electrode and RFA techniques.

Beam neutralization	B, C and S on	B, C off and S on	B, C and S off
Clear. Electrodes	7.3 %	25.2 %	89.2 %
RFA	7.3 %	27.5 %	79.5 %

The CCD camera can be placed before, between and after the quadrupole magnets. It is an optical diagnostic that provides time-resolved 4-D transverse information from the beam hitting a kapton scintilator. Beam focusing to small spots has been seen and attributed to ECE. From side measurements of beam interaction with desorbed gas we inferred an average velocity of desorbed gas of 0.5 mm/μs [26], consequently, during the beam duration of 5 μs, most of the gas cloud does not expand into the beam path, and it will not be ionized.

One Faraday cup is positioned before and another after the magnetic section. They are intercepting diagnostics that have two electrodes, a suppressor ring upstream and a collector with a honeycomb structure downstream, that are inside a grounded case for electrical shielding. The current difference measured before and after the magnetic section provides beam losses. For a fill factor of 60%, the measured current loss is ~ 2 mA. As the total measured beam-background gas interaction cross section (ionization plus charge exchange) with the RFA is 1.6×10^{-20} m^2 [27], giving an upper limit to the beam neutralization at the end of the pulse of 0.3 %, the major electron source will be from ion beam losses to the walls.

4. CONCLUSIONS

Electrostatic quadrupoles provide efficient ion-beam transport at low energy and provide clearing fields that sweep out unwanted electrons. At higher energies the transport is usually by quadrupole magnets. HCX is studying high-line-charge-density, high-perveance beam transport by quadrupole magnets for application to high-energy-density physics and to heavy-ion fusion.

At this regime space-charge forces strongly influence the beam properties. Electron clouds are a ubiquitous source of negative charge that alters of the space-charge forces, which can change beam emittance, envelope size, and halo, and can drive instabilities.

The HCX is highly instrumented to measure sources and accumulation of electrons in the magnetic section. The signal intensities collected on the wall electrodes within the last two magnetic quadrupoles are calibrated with data from GESD experiment to determine ion-beam and electron behavior inside the magnets. Clearing electrodes, RFA and suppressor are placed between and at the end of the magnets, with these and the other diagnostics discussed, we study the electron cloud, comparing the results with state-of-art simulations, and develop a non-intrusive technique that measures the time-dependent electron cloud density during the beam [21].

Future plans include the installation of an electron gun for studies of electron transport, accumulation, and effects on the beam. During the beam pulse, the magnetic section forms an electron trap that can accumulate electrons, if the suppressor and the last electrostatic quadrupole are biased. The beam space-charge potential and the adjustable potential energy of the gun-extracted electrons, given by the cathode bias, will enable us to change the electron spatial distribution during the K+ beam pulse, providing a controllable source of electrons that can be measured with HCX diagnostics.

ACKNOWLEDGEMENT

We wish to thank Tak Katayanagi who built the diagnostics, Wayne G. Greenway, Larry W. Mills and Gary Ritchie who maintain HCX, and Craig Rogers, Ed Romero and William L. Waldron who provided electronic support. We also want to express our gratitude to Richard A. Rosenberg and Katherine C. Harkay for sharing details that aided our RFA design, and to Miguel Furman for his insightful comments. This work was performed under the auspices of U.S.

Department of Energy by the University of California, LLNL and LBNL under contracts No. W-7405-ENG-48, and No. DE-AC02-05CH11231.

[1] L. R. Prost et al., Nucl. Instrum. Methods Phys. Res. A **544**, 151(2005).

[2] H. Fukuma, in: Proc. of Diag. Instrum. Part. Acc. Conf., Lyon, France, 2005, p. 122.

[3] G. Budker, G. Dimov, and V. Dudnikov, Sov. Atom. E. **22**, 5 (1967).

[4] O. Gröbner, in *Proceedings of the 10th International Conference on High-Energy Accelerators, Protvino, Russia* (Institute of High Energy Physics, Protvino, 1977), p. 277.

[5] R. J. Macek et al., in: Proc. of Part. Acc. Conf., Chicago, IL, 2001, p. 688.

[6] S. Y. Zhang et al., in: Proc. of Eur. Part. Acc. Conf., Lucerne, 2004, p. 944.

[7] M. Izawa, Y. Sato, and T. Toyomasu, Phys. Rev. Lett. **74**, 5044 (1995).

[8] K. Ohmi, Phys. Rev. Letters **75**, 1526 (1995).

[9] J. W. Flanagan et al., Phys. Rev. Lett. **94**, 054801 (2005).

[10] W. T. Weng et al., in: Proc. of Part. Acc. Conf., Vancouver, 1999, p. 970.

[11] R. J. Macek, and A. Browman, in: Proc. of Part. Acc. Conf., Knoxville, TN, 2005, p. 2547.

[12] M. A. Furman, LBNL Report No. 50765, 2002.

[13] J.-L. Vay et al., in: Proc. of Part. Acc. Conf., Knoxville, TN, 2005, p. 525.

[14] R. H. Cohen et al., Phys. Rev. ST Accel. Beams **7**, 124201 (2004).

[15] J. P. Boris, in *Proceedings of the 4th International Conference on Numerical Simulation of Plasmas, Washington, DC, 1970* (Naval Research Laboratory, Washington, DC, 1971), U.S. Government Printing Office, stock number 0851_00059, p. 3.

[16] J.-L. Vay et al., Phys. Plasmas **11**, 2928 (2004).

[17] A. W. Molvik et al., Phys. Rev. ST Accel. Beams **7**, 093202 (2004).

[18] M. Kireeff Covo et al., Phys. Rev. ST Accel. Beams **9**, 063201 (2006).

[19] M. Kireeff Covo, AVS 53rd International Symposium, VT-WeM5, contributed talk.

[20] A.W. Molvik et al., Nucl. Instrum. Methods Phys. Res. A **544**, 194 (2005).

[21] M. Kireeff Covo et al., Phys. Rev. Lett. **97**, 054801 (2006).

[22] R. H. Cohen et al., LBNL Report No. 56496, 2004.

[23] R. A. Rosenberg, and K. Harkay, Nucl. Instrum. Methods Phys. Res. A **453**, 507 (2000).

[24] M. Kireeff Covo et al, submitted to Nucl. Instrum. Methods Phys. Res. A.

[25] J. Klabunde et al., in: Proc. of Part. Acc. Conf., Santa Fe, NM, 1983, p. 2543.

[26] F. M. Bieniosek, to be published.

[27] M. Kireeff Covo, to be published.